

## Phase diagram of the Weeks-Chandler-Andersen potential from very low to high temperatures and pressures

Alauddin Ahmed and Richard J. Sadus\*

*Centre for Molecular Simulation, Swinburne University of Technology, P.O. Box 218, Hawthorn, Victoria 3122, Australia*

(Received 21 September 2009; published 1 December 2009)

A combination of two molecular simulation algorithms has been used to determine the solid-liquid coexistence of the Weeks-Chandler-Andersen (WCA) fluid from low temperatures up to very high temperatures. Values are reported for the coexistence pressure, temperature, energy, enthalpy change, and densities of both the liquid and solid phases. At very high temperatures, the coexistence pressure approaches the same 12th-power soft-sphere asymptote as the 12–6 Lennard-Jones potential. However, in contrast to the Lennard-Jones potential, which shows a discontinuity of pressure at low temperatures, the coexistence pressure of the WCA potential approaches the zero-temperature limit. Empirical relationships are determined to accurately reproduce the coexistence pressure and both solid and liquid phase densities from near zero temperature to very high temperatures. The simulation data are used to improve the accuracy of a WCA equation of state. The validity of common melting and freezing rules is tested.

DOI: [10.1103/PhysRevE.80.061101](https://doi.org/10.1103/PhysRevE.80.061101)

PACS number(s): 64.10.+h, 61.20.Ja, 64.70.D-, 71.15.Pd

### I. INTRODUCTION

The Weeks-Chandler-Andersen [1] (WCA) potential is commonly used as part of a broader model for molecular fluids such as polymers [2,3] and dendrimers [4,5]. It can be applied to both bonded and nonbonded interactions and it forms the basis of many liquid state theories [6–8]. The utility of the potential is that it provides a simpler alternative to the Lennard-Jones (LJ) potential that is more realistic than a crude hard-sphere potential. It possesses many of the physical attributes of the Lennard-Jones system. However, a key difference is that the WCA potential is limited to solid-liquid equilibria. The absence of vapor-liquid equilibria means that there are no critical or triple points.

Despite its important role in liquid state theories and molecular simulation, relatively few data are available for solid-liquid equilibria for the WCA potential [9,10]. In contrast, there are extensive simulation data [11–15] for the solid-liquid coexistence of Lennard-Jones fluids. The two previous investigations [9,10] of WCA solid-liquid coexistence have been performed for either a single state point or for a limited temperature range. de Kuijper *et al.* [10] obtained the WCA melting line from Monte Carlo (MC) simulations, whereas Hess *et al.* [9] approximately located the solid-liquid phase coexistence for one temperature using canonical ( $NVT$ ) and isothermal-isobaric ( $NpT$ ) molecular dynamics (MD) algorithms. The freezing point densities and pressures obtained for the two MD simulation methods showed discrepancies of 5% and 18.5%, respectively, whereas the different simulations were in good agreement for the melting point properties. Although the freezing point densities and pressures from both MC and  $NVT$  MD simulations are in agreement, there is a discrepancy of 5.2% and 15.5% for the melting point density and pressure, respectively. These discrepancies are somewhat surprising because, unlike the Lennard-Jones potential, solid-liquid coexistence for the WCA potential is not

affected by cutoff errors that can contribute as much as 10% to the properties [13].

The aim of this work is to provide a comprehensive description of the solid-liquid equilibria of the WCA fluid. We report data for the phase diagram using the algorithm of Ge *et al.* [14] and the Gibbs-Duhem integration (GDI) [15] technique. The conjecture [16,17] of abnormal behavior at low temperatures is investigated by examining the melting behavior at very low temperatures. We also trace the melting line of the WCA potential to very high temperatures to test the hypothesis that it approaches a 12th-power soft-sphere asymptote. An improved WCA equation of state and three empirical expressions for the solid-liquid coexistence pressure, freezing density, and melting density are reported.

### II. THEORY

#### A. Weeks-Chandler-Andersen potential

That WCA potential [1] is the LJ potential truncated at the minimum potential energy at a distance  $r_{ij}=2^{1/6}\sigma$  on the length scale and shifted upward by the amount  $\varepsilon$  on the energy scale such that both the energy and force are zero at or beyond the cutoff distance:

$$u(r_{ij}) = \begin{cases} 4\varepsilon \left[ \left( \frac{\sigma}{r_{ij}} \right)^{12} - \left( \frac{\sigma}{r_{ij}} \right)^6 \right] + \varepsilon, & r \leq 2^{1/6}\sigma \\ 0, & r > 2^{1/6}\sigma, \end{cases} \quad (1)$$

where  $\varepsilon$  and  $\sigma$  are the characteristic energy and distance parameters, respectively. Equation (1) is a purely repulsive potential.

The intermolecular parameters are used to define the reduced density ( $\rho^* = \rho\sigma^3$ ), reduced temperature ( $T^* = kT/\varepsilon$ ), reduced energy ( $E^* = E/\varepsilon$ ), reduced pressure ( $p^* = p\sigma^3/\varepsilon$ ), and reduced time ( $\tau^* = [\varepsilon/m\sigma^2]^{1/2}\tau$ ). All quantities quoted in this work are in terms of these reduced quantities and the asterisk superscript and the prefix “reduced” will be omitted in the rest of the paper.

\*rsadus@swin.edu.au

## B. Simulation details

Since our simulations covered a wide range of temperatures and densities we had to carefully choose the integration time step for different state points such that the time step was small enough to solve the equations of motion correctly and large enough to sample phase space adequately [18]. To do this we carried out short simulations to approximately locate solid-liquid phase coexistence for selected temperatures using the same integration time step of 0.001. Thereafter, to determine the appropriate time step for any given temperature, we performed *NVE* simulations at ten random densities around the approximate phase coexistence density to observe the conservation of total energy. An order of  $10^{-4}$  fluctuations in total energy ensures the correct choice of time step [18].

All simulation trajectories were typically run for  $2 \times 10^5$  time steps. The first  $5 \times 10^4$  time steps of each trajectory were used either to equilibrate zero-shearing field equilibrium molecular dynamics (EMD) or to achieve nonequilibrium steady state after the shearing field is switched on. The rest of the time steps in each trajectory were used to accumulate the average values of thermodynamic variables and standard deviations.

To obtain the most accurate results for any given temperature, different simulation algorithms were used for different ranges of temperature. It is convenient to identify three different ranges of temperature. The low temperature region is from  $T \rightarrow 0$  to the Lennard-Jones triple point temperature of  $T=0.68$ . Intermediate temperatures are  $0.68 < T < 2.74$ , whereas  $T > 2.74$  are high temperatures.

### 1. Simulations at low and intermediate temperatures

At low and intermediate temperatures, the solid-liquid phase coexistence properties were obtained using the algorithm reported by Ge *et al.* [14] that combines the techniques of both EMD and nonequilibrium molecular dynamics (NEMD) simulations. As discussed elsewhere [14,19] NEMD was used to determine the pressure at different strain rates for a common temperature and density. The algorithm is based on an empirical observation of the strain-rate behavior of pressure. At densities equal to or greater than the freezing point, there is an abrupt change in pressure between the zero strain-rate case and the first nonzero strain rate, which allows us to accurately identify the freezing density and pressure. Having identified the freezing point, EMD calculations are performed to obtain the isothermal pressure-density behavior of the solid curve. The density of the melting point is the point at which the constant pressure tie line touches the solid curve. The algorithm has been extensively investigated [20] for Lennard-Jones fluids.

The initial configuration in all the simulations was a face-centered-cubic (fcc) lattice structure. The isothermal isochoric NEMD simulations were performed by applying the standard *slld* equations [21] of motion for planar Couette flow coupled with Lees-Edwards [14,21] periodic boundary conditions. If the applied strain rate is switched off in the *slld* algorithm it behaves like Newton's equations of motion and NEMD converts to EMD. The *NVT* EMD simulations were performed using conventional cubic periodic boundary

conditions. In these molecular dynamics simulations a Gaussian thermostat multiplier [22] was used to keep the kinetic temperature of the fluid constant. The equations of motion were integrated with a five-value Gear predictor-corrector scheme [23].

We performed a wide range of simulations for locating the solid-liquid phase transitions with a 0.01 increment in densities. For each state point we have carried out three simulations, one for zero strain-rate equilibrium molecular dynamics and normally two for strain rates of 0.1 and 0.2. In principle, only the difference between the 0 and 0.1 strain-rate isothermal-isochoric simulation is sufficient to detect the phase transitions. To clarify the issue of solidlike and liquidlike metastable states we performed additional simulations for the 0.2 strain rate.

For temperatures  $0.0001 < T \leq 0.01$  we used a density interval 0.01 and strain rates of 0.01 and 0.02. At these very low temperatures, the higher strain rates of 0.1 and 0.2 did not exhibit the necessary pressure jump for locating the solid-liquid phase transition. We conducted test runs on WCA liquid at low temperatures with different strain rates to check for strain rate independent Couette flow behavior. Alternatively, the choice of strain rates could be obtained from a stability analysis at a given temperature and density [24]. The melting point density is accurate to within the limit of the density change, whereas the accuracy of the freezing point density is 0.01.

### 2. Simulations at high temperatures

The solid-liquid coexistence properties at high temperatures were obtained using the GDI algorithm. The GDI algorithm is not self-starting. The starting point required by the GDI method was obtained from the results at intermediate temperatures described above. The Clapeyron equation used in the evaluation of the GDI series is related to the stability of the integration at a given temperature [15]. For the Lennard-Jones potential, it has been reported [15] that two different versions of the Clapeyron equation must be used below and above  $T=2.74$  to maintain the stability of the integration. The starting point of  $T=2.74$  was used for the high temperature GDI simulations without any further rigorous testing of the GDI series for the WCA potential.

At the beginning of the simulation 932 atoms were distributed between boxes to represent solid and liquid phases. The box in the liquid phase contained 432 atoms while the box in the solid phase contained 500 atoms in the face-centered-cubic lattice structure. The simulations were performed in cycles. A simulation period of 20 000 was used to accumulate the simulation averages followed by an equilibration period of 20 000 cycles. In all the GDI series of simulations, the temperature change per step in the decreasing direction was  $\Delta\beta=0.03$ , where  $\beta$  is the reciprocal of the temperature.

### 3. Finite-size effects

The system size dependency of the solid-liquid phase coexistence pressure, temperature, and densities for the WCA

TABLE I. Coexistence pressures and melting and freezing densities of a WCA fluid at  $T^*=1.00$  for different numbers of particles.

| $N$   | $p^*$  | $\rho_{liq}^*$ | $\rho_{sol}^*$ |
|-------|--------|----------------|----------------|
| 108   | 11.195 | 0.93           | 0.99           |
| 256   | 12.014 | 0.94           | 1.01           |
| 864   | 13.127 | 0.96           | 1.03           |
| 2048  | 12.577 | 0.95           | 1.016          |
| 4000  | 12.576 | 0.95           | 1.016          |
| 13500 | 13.097 | 0.96           | 1.03           |
| 32000 | 13.058 | 0.96           | 1.03           |
| 62500 | 13.061 | 0.96           | 1.03           |

system are not known. For the Lennard-Jones potential thermodynamic variables can vary from 3% to 6% depending on the system size [13,25] and we can also expect similar size effects for the WCA system. To test for the effect of system size on our results, we performed simulations at temperatures of  $T=1.00$  for  $N=108, 256, 864, 2048, 4000, 13\,500,$  and  $62\,500$  and the results are summarized in Table I. The maximum variation of the coexistence pressure is 14.3%, whereas a maximum variation of 3.1% is observed for the coexistence densities. The effect of system size does not appear to scale with  $1/N$ . Using  $N=4000$  represents a reasonable compromise between maintaining accuracy and minimizing computational effort.

### III. RESULTS AND DISCUSSION

#### A. Solid-liquid coexistence

The WCA simulation data for low to intermediate temperatures and high temperatures are summarized in Tables II and III, respectively. Solid-liquid coexistence data for the WCA potential have only been reported previously [10] at  $T=0.5, 0.75, 1.0, 1.25, 1.5, 2.0,$  and  $5.0$ . A comparison of our data with literature data for the pressure and coexisting liquid and solid densities is given in Fig. 1. The relative difference between our calculations and literature data is quantified in

TABLE II. Solid-liquid phase coexistence properties of the WCA potential at low to intermediate temperatures. Values in parentheses represent the uncertainty in the last digit.

| $T^*$ | $p^*$     | $\rho_{liq}^*$ | $E_{liq}^*$  | $\rho_{sol}^*$ | $E_{sol}^*$  | $\Delta h^*$ |
|-------|-----------|----------------|--------------|----------------|--------------|--------------|
| 0.001 | 0.0068(3) | 0.65           | $6.5E-5(4)$  | 0.7            | $5.9E-5(4)$  | 0.00076      |
| 0.003 | 0.0217(7) | 0.66           | $3.4E-4(1)$  | 0.72           | $3.1E-4(1)$  | 0.00278      |
| 0.006 | 0.045(1)  | 0.67           | $9.8E-4(4)$  | 0.735          | $8.8E-4(4)$  | 0.00607      |
| 0.009 | 0.069(1)  | 0.68           | $18.1E-4(7)$ | 0.744          | $16.2E-4(6)$ | 0.00904      |
| 0.01  | 0.077(1)  | 0.68           | $21.1E-4(8)$ | 0.74           | $18.5E-4(7)$ | 0.00954      |
| 0.05  | 0.439(6)  | 0.73           | $22.7E-3(5)$ | 0.8            | 0.0201(5)    | 0.05534      |
| 0.1   | 0.94(1)   | 0.76           | 0.062(1)     | 0.833          | 0.054(1)     | 0.11700      |
| 0.2   | 2.03(2)   | 0.80           | 0.166(2)     | 0.87           | 0.141(2)     | 0.22884      |
| 0.3   | 3.14(3)   | 0.83           | 0.285(4)     | 0.90           | 0.248(4)     | 0.33166      |
| 0.4   | 4.37(4)   | 0.85           | 0.427(6)     | 0.92           | 0.364(6)     | 0.45545      |
| 0.5   | 5.60(5)   | 0.87           | 0.574(7)     | 0.94           | 0.492(7)     | 0.56269      |
| 0.6   | 6.95(5)   | 0.89           | 0.737(9)     | 0.96           | 0.633(9)     | 0.67325      |
| 0.7   | 8.42(6)   | 0.91           | 0.91(1)      | 0.98           | 0.78(1)      | 0.78951      |
| 0.8   | 9.60(7)   | 0.92           | 1.07(1)      | 0.99           | 0.92(1)      | 0.88071      |
| 0.9   | 11.28(8)  | 0.94           | 1.27(1)      | 1.00           | 1.07(1)      | 0.92090      |
| 1.0   | 12.57(9)  | 0.95           | 1.44(1)      | 1.016          | 1.24(1)      | 1.05865      |
| 1.15  | 15.5(1)   | 0.98           | 1.80(1)      | 1.05           | 1.57(1)      | 1.28860      |
| 2.00  | 30.4(1)   | 1.07           | 3.72(3)      | 1.14           | 3.31(3)      | 2.15879      |
| 2.74  | 45.1(2)   | 1.13           | 5.60(4)      | 1.20           | 5.04(5)      | 2.89380      |

Fig. 2. For  $T=0.50$  the reported pressure, freezing density, and melting density are approximately 13.1%, 3.3%, and 3.0% higher, respectively, than our results. For  $T=1.25$  our pressure is 1.9% higher than reported elsewhere. The differences in pressure at  $T=1.5$  and  $T=2.0$  are approximately 3% and 5.9%, respectively.

As discussed above and illustrated in Table IV, there are considerable discrepancies in the literature between the values previously reported by other workers for  $T=1.0$ . At this temperature, our liquid density is in good agreement with the values reported for either  $NVT$  MD [9] or MC [10] simulations, which in turn is higher than  $NpT$  MD [9] calculations. Our solid density also agrees reasonably well with  $NVT$  MC data, which is higher than either  $NVT$  or  $NpT$  MD simula-

TABLE III. Solid-liquid phase coexistence properties of the WCA potential at high temperatures. Values in parentheses represent the uncertainty in the last digit.

| $T^*$    | $p^*$    | $\rho_{liq}^*$ | $E_{liq}^*$ | $\rho_{sol}^*$ | $E_{sol}^*$ | $\Delta h^*$ |
|----------|----------|----------------|-------------|----------------|-------------|--------------|
| 3.63636  | 66.327   | 1.165(1)       | 7.21(2)     | 1.218(1)       | 6.31(1)     | 3.033        |
| 4.08163  | 77.605   | 1.198(1)       | 8.72(2)     | 1.252(1)       | 7.73(2)     | 3.376        |
| 4.65116  | 92.632   | 1.237(1)       | 10.65(2)    | 1.294(1)       | 9.53(3)     | 3.795        |
| 5.40540  | 113.476  | 1.286(1)       | 13.29(3)    | 1.342(1)       | 12.04(4)    | 4.364        |
| 6.45161  | 143.809  | 1.342(1)       | 17.08(3)    | 1.401(1)       | 15.62(3)    | 4.969        |
| 8.00000  | 191.135  | 1.415(2)       | 22.78(4)    | 1.475(1)       | 21.04(4)    | 5.973        |
| 10.52631 | 274.739  | 1.514(2)       | 32.46(7)    | 1.576(1)       | 30.29(5)    | 7.159        |
| 15.38461 | 450.978  | 1.662(2)       | 51.6(1)     | 1.729(1)       | 48.55(7)    | 9.311        |
| 28.57142 | 1021.973 | 1.924(5)       | 109.2(2)    | 2.000(3)       | 103.3(2)    | 23.769       |

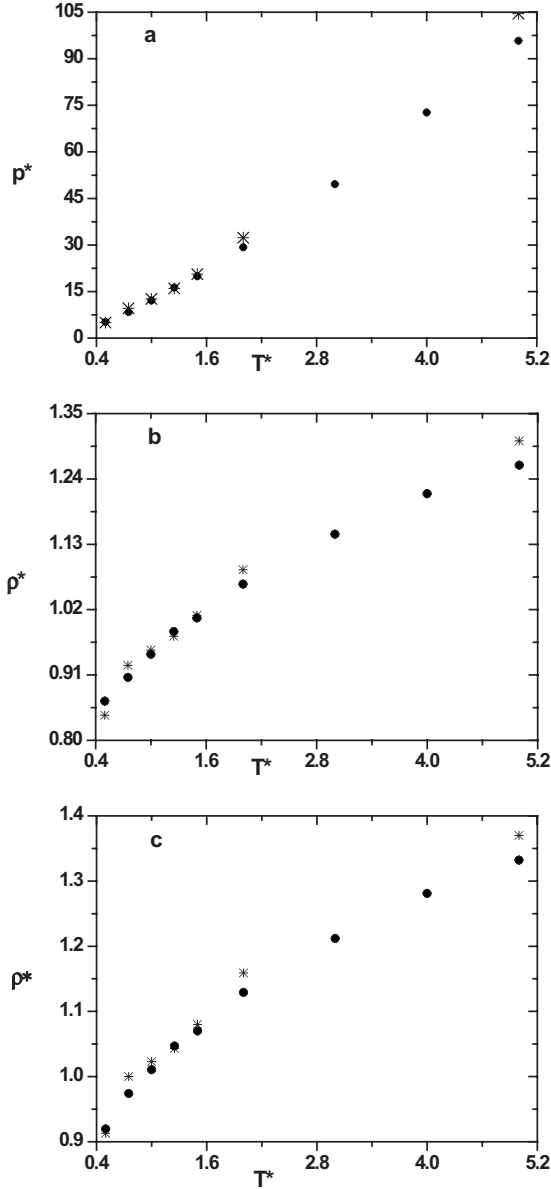


FIG. 1. Comparison of the solid-liquid coexistence (a) pressure, (b) liquid densities, and (c) solid densities for the WCA potential calculated in this work (●) with data from literature (\*, [10]). The errors are approximately equal to the symbol size.

tions. The liquid phase pressure is in agreement with either the  $NVT$  MC or MD calculations, which is higher than the  $NpT$  MD simulations. In view of this, our MD results clearly resolve the discrepancy in the literature in favor of the  $NVT$  MC [10] data.

The solid-liquid phase diagram is illustrated in Fig. 3. It is apparent from Fig. 3(b) that the difference between liquid and solid densities is relatively small at low temperatures but progressively increases with increasing temperature.

The effect of intermolecular interactions on the two phases can be quantified in terms of either the relative density difference (r.d.d.) and the fractional density change (f.d.c.) at freezing (also known as the miscibility gap). The r.d.d. is defined as [9]  $\delta n = 2(\rho_{sol} - \rho_{liq}) / (\rho_{sol} + \rho_{liq})$ , where  $\rho_{sol}$  and  $\rho_{liq}$  are the solid and liquid densities of the system at

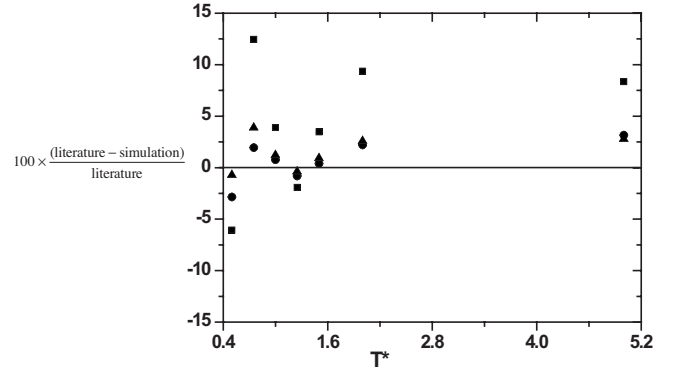


FIG. 2. Comparison of the relative percentage difference in pressure (■), liquid density (●), and solid density (▲) at different temperatures obtained in this work and data available from the literature [10].

solid-liquid coexistence. The miscibility gap or f.d.c. is defined as [15,26]  $(\rho_{sol} - \rho_{liq}) / \rho_{liq}$ . The lower bound of the relative density difference is 0.037, which corresponds approximately to 12-inverse-power soft spheres [27] and the upper bound value is 0.098, which is the value for hard spheres [17].

The temperature dependency of the r.d.d. and f.d.c. is illustrated in Fig. 4. It is evident that both metrics decrease with increasing temperature. A comparison is also made in Fig. 4 with the LJ potential. It is apparent that the values obtained for the WCA are lower than the LJ values in all cases. The average relative density difference of the LJ system from Agrawal and Kofke's data is 0.093 compared with 0.060 obtained from our data, which lies between the hard-sphere and  $r^{-12}$  soft-sphere values. For  $T=1$  Hess *et al.* [9] and de Kuijper *et al.* [10] reported  $\delta n \approx 0.063$  and  $\delta n \approx 0.0718$ , respectively. This compares to  $\delta n \approx 0.067$  obtained from our data.

## B. Low and high temperature limits

It is expected that at high temperatures the average kinetic energy will be such that it would be impossible to distinguish between LJ and WCA interactions. de Kuijper *et al.* [10] predicted that this would occur at  $T > 10$ . We have calculated solid-liquid coexistence for temperatures up to  $T=28.57$  and these data are compared with results for the Lennard-Jones potential in Fig. 5(a). It is apparent from this comparison that the WCA and LJ results begin to converge at high temperatures. Both the WCA and LJ calculations show convergence

TABLE IV. Comparison of WCA solid-liquid coexistence data at  $T^*=1.0$  with literature data using various simulation techniques as discussed in the text.

| Method    | $N$  | $P_{liq}^*$ | $\rho_{liq}^*$ | $P_{sol}^*$ | $\rho_{sol}^*$ |
|-----------|------|-------------|----------------|-------------|----------------|
| $NVT$ MC  | 500  | 12.60       | 0.952          | 12.60       | 1.023          |
| $NVT$ MD  | 2048 | 12.62       | 0.960          | 10.65       | 0.970          |
| $NpT$ MD  | 8788 | 10.65       | 0.912          | 10.67       | 0.971          |
| This work | 4000 | 12.57       | 0.950          | 12.57       | 1.016          |

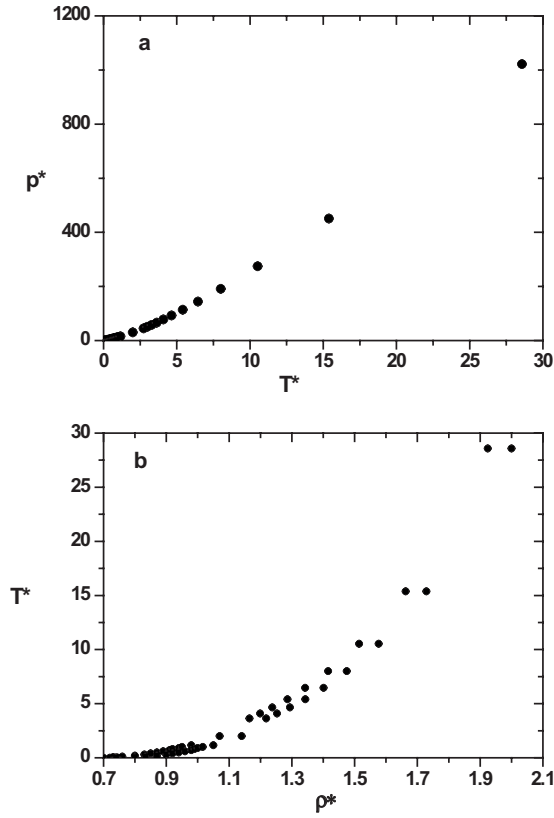


FIG. 3. Solid-liquid coexistence (a) pressure (●) and (b) freezing (upper points) and melting (lower points) densities (●) as a function of temperature.

to a common asymptote [15] at  $1/T \rightarrow 0$  which corresponds to the 12th-power soft-sphere limit.

In contrast to the high temperature behavior, Fig. 5(b) indicates that the WCA and LJ fluids behave very differently as  $T \rightarrow 0$ . A clear divergence in the pressure-temperature behavior of the two potentials is evident for  $T < 1.0$ . There is an apparent discontinuity [15] in pressure for the LJ potential, which stops short of approaching  $T=0$ . In contrast, the WCA calculation approaches  $T=0$ . At  $T \approx 0$ , we estimate that the pressure is  $p_0^{WCA} < 0.0068$ .

**C. Temperature dependence of coexistence pressure and densities**

Using the special scaling properties of the inverse  $n$ th-power potential, Agrawal and Kofke [15] obtained the following relationship for the solid-liquid coexistence pressure of a 12–6 Lennard-Jones fluid:

$$\left. \begin{aligned} \rho_{liq} &= \beta^{-5/4} \exp(-0.51\beta^{2/5})(0.027 + 1.47\beta + 0.12\beta^2 + 1.4 \times 10^{-4}\beta^3 + 1.94 \times 10^{-6}\beta^4) \\ \rho_{solid} &= \beta^{-5/4} \exp(-0.51\beta^{2/5})(0.027 + 1.55\beta + 0.14\beta^2 + 1.1 \times 10^{-4}\beta^3 + 2.1 \times 10^{-6}\beta^4) \end{aligned} \right\} \quad (4)$$

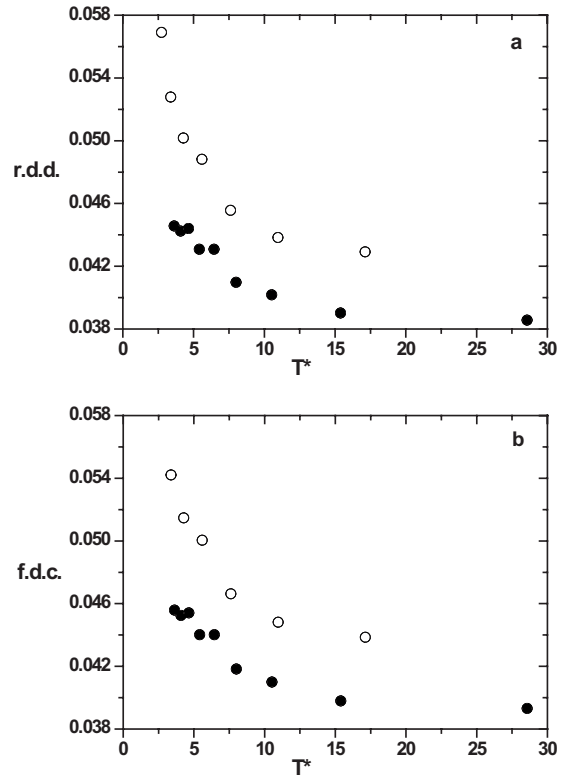


FIG. 4. Comparison of (a) r.d.d. and (b) f.d.c. WCA data as a function of temperature obtained in this work (●) with Lennard-Jones (○) data from the literature [15].

$$p_{12-6} = \beta^{-5/4} \exp(-D\beta^{1/2})(16.89 + k_1\beta + k_2\beta^2), \quad (2)$$

where  $\beta = 1/kT$ , 16.89 is the limiting soft-sphere value of  $p\beta^{5/4}$ ,  $D=0.4759$  was determined from soft-sphere simulation data, and  $k_1$  and  $k_2$  are fitting parameters. The fact that the WCA fluid has the same (Fig. 6) soft-sphere high temperature limiting behavior as the LJ potential means that it should be possible to fit Eq. (2) to our data. However, unlike the LJ potential the WCA pressure is continuous until  $T=0$  and there is no triple point, which means a fit can be made for the entire temperature range. For the WCA fluid, we found that the introduction of an additional parameter ( $k_0$ ) was required to account for these differences:

$$p_{WCA} = \beta^{-5/4} \exp(-D\beta^{1/2})(16.89k_0 + k_1\beta + k_2\beta^2). \quad (3)$$

When  $k_0=2.34$ ,  $k_1=-59$ , and  $k_2=12$ , Eq. (3) accurately reproduces the pressure-temperature behavior as evident from a squared correlation coefficient ( $R^2$ ) value of 0.99.

Van der Hoef [28] fitted the freezing and melting densities for a 12–6 Lennard-Jones via two polynomial relationships involving  $\beta$ . We fitted our WCA data via the following relationships:

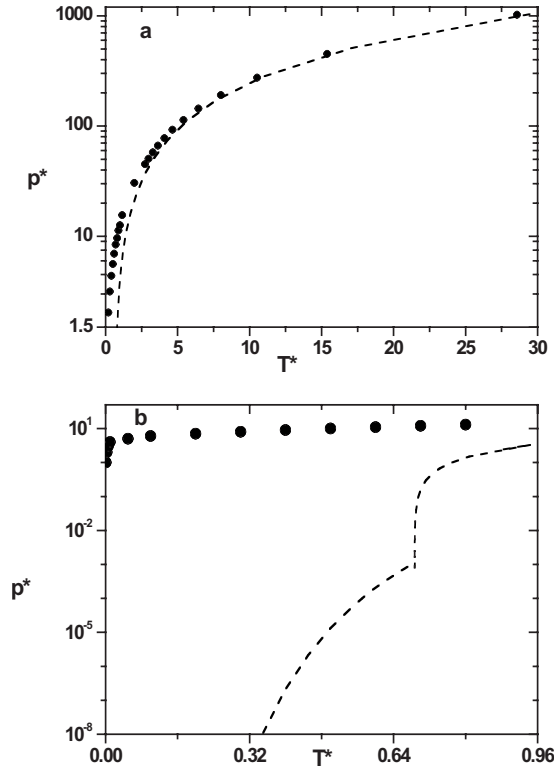


FIG. 5. Comparison of (a) the overall pressure-temperature and the (b) pressure–low temperature behavior of the WCA fluid calculated in this work (●) with literature data [15] for the Lennard-Jones potential (---). The Lennard-Jones data were supplemented by calculations using Eq. (1) from Ref. [28].

In Eq. (4) we have introduced an exponential term to Van der Hoef’s original formulas to accommodate the low temperature behavior of the WCA fluid. We found that the WCA

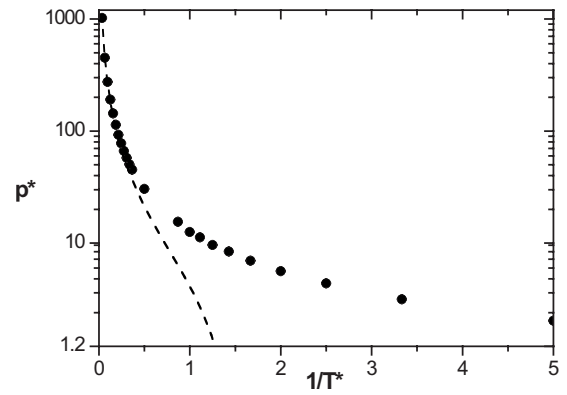


FIG. 6. Comparison of the solid-liquid coexistence pressure of the WCA potential (●) with data reported for the LJ potential (---) [15] as a function of reciprocal temperature.

simulation data could be accurately ( $R^2=0.99$ ) fitted to these equations.

#### D. Comparison with equation of state calculations

Attempts [29–31] have been made to develop an equation of state for the WCA potential. The usual starting point is a variation of the Carnahan-Starling [32] equation, which provides an accurate description of the compressibility factor of hard spheres ( $Z$ ) in terms of the packing fraction of hard spheres ( $y = \pi\rho\sigma^3/6$ ):

$$Z = \frac{1 + y + ay^2 - by^3}{(1 - y)^3}, \quad (5)$$

where  $a$  and  $b$  are adjustable parameters. When  $a=b=1$ , Eq. (5) is the original Carnahan-Starling equation. A WCA equation of state is obtained by simply substituting the hard-sphere diameter with a temperature-dependent formula:

$$\left. \begin{aligned} \sigma &= \frac{2^{1/6}}{(1 + \sqrt{T})^{1/6}} \\ \sigma &= \frac{0.3837T + 1.068}{0.4293T + 1} \\ \sigma &= 0.111\,175\,24T^{-1} - 0.076\,383\,859T^{-0.5} \\ &\quad + 1.080\,142\,48 + 0.000\,693\,129T^{0.5} \\ &\quad - 0.063\,920\,968 \log T \end{aligned} \right\} \begin{array}{l} \text{Heyes and Okumura } (a = 3.597, b = 5.836) \\ \text{Verlet and Weis } (a = b = 1) \\ \text{Kolafa and Nezbeda } (a = b = 1) \end{array} \quad (6)$$

Figure 7 compares the compressibility factor predicted by these WCA equations of state with our data for the freezing line at different temperatures. It is apparent from this comparison that the Kolafa and Nezbeda [31] and Verlet and Weis [30] equations fail to even qualitatively reproduce the variation of the compressibility factor with respect to temperature. The Heyes and Okumura equation [29] yields qualitative agreement for the compressibility factors at all

temperatures. The average absolute deviation between the compressibility factors predicted by the Heyes and Okumura equation and our simulation data is 8.5%. In view of this reasonably good quantitative agreement, we used our simulation data to reevaluated the  $a$  and  $b$  parameters of the Heyes and Okumura equation. Values of  $a=17.22$  and  $b=31.1$  result in an average absolute deviation of approximately 0.38% and good agreement at all temperatures (Fig. 7). This sug-

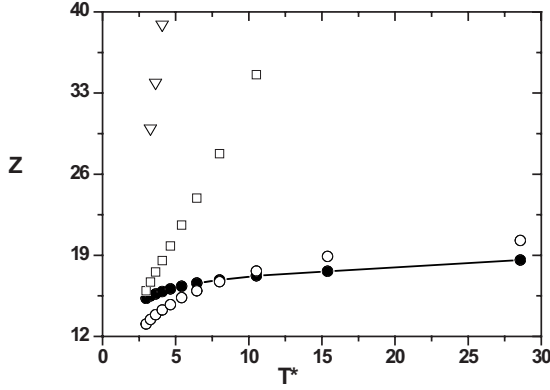


FIG. 7. Comparison of molecular simulation data for the compressibility factors of the WCA fluid obtained in this work (●) with calculations using the Heyes and Okumura (○), Verlet and Weis EOS (□), and Kolafa and Nezbeda (▽) equations of state. The solid line represents calculations of the reparametrized Heyes and Okumura equation reported here.

gests that the reparametrized Heyes and Okumura equation could have a role in equation of state development for real fluids as an alternative to the Carnahan-Starling hard-sphere term.

**E. Melting and freezing rules**

A commonly used method to predict melting is the Lindemann rule [33] which states that a solid melts if the root-mean-square displacement of particles around their ideal position is approximately 10% of their nearest-neighbor distance. Luo *et al.* [34] reported that the Lindemann rule is valid for the Lennard-Jones potential for a wide range of pressures. In view of this, it is reasonable for it to also apply to WCA fluids. Ashcroft *et al.* [35] showed that, when viewed from the liquid side of the phase transition, Lindemann’s melting rule can be expressed as  $L = \sigma_{HS}(T)^3 / V_m = \text{const}$ , where  $V_m$  is equal to the volume of the liquid and  $\sigma_{HS}(T)$  is the temperature-dependent hard-sphere diameter. Heyes and Okumura [29] have found that a good approximation for the effective hard-sphere diameter of the WCA potential is  $\sigma_{HS}(T) = 2^{1/6} / (1 + \sqrt{T})^{1/6}$ . Values of  $L$  obtained from our simulation data at various temperatures are summarized in Table V. It is evident that  $L$  is close to being constant for most temperatures.

Raveché *et al.* [36] proposed that the ratio of the first maximum to the nonzero first minimum of the radial distribution function on the freezing line is constant [ $G = g(r_{\text{max}}) / g(r_{\text{min}}) = \text{const}$ ]. Figure 8(a) compares the radial distribution functions at melting and freezing densities. We have calculated values of  $G$  for the freezing densities at low and intermediate temperatures and the results are summarized in Table V. Although there is some variability in the value of  $G$ , it can be used as a reasonable indicator of freezing.

We have also tested the Hansen and Verlet [11] freezing rule, which says that upon freezing the structure factor has a maximum value of  $S(k_0) = 2.85$ . We have obtained the structure factor via a Fourier transformation of the pair-

TABLE V. Invariants of the Lindemann, Raveché *et al.*, and Hansen and Verlet melting or freezing rules as a function of coexistence temperature.

| $T^*$ | $L = \sigma_{SH}(T^*)^3 / V_m$ | $G = g(r_{\text{max}}) / g(r_{\text{min}})$ | $S(k)$ |
|-------|--------------------------------|---|--------|
| 0.1   | 1.106                          | 0.136                                       | 3.10   |
| 0.2   | 1.095                          | 0.204                                       | 3.02   |
| 0.3   | 1.084                          | 0.151                                       | 2.97   |
| 0.4   | 1.080                          | 0.160                                       | 2.90   |
| 0.5   | 1.081                          | 0.165                                       | 2.86   |
| 0.6   | 1.084                          | 0.168                                       | 2.83   |
| 0.7   | 1.077                          | 0.168                                       | 2.80   |
| 0.8   | 1.084                          | 0.175                                       | 2.76   |
| 0.9   | 1.080                          | 0.173                                       | 2.75   |
| 1     | 1.100                          | 0.174                                       | 2.70   |
| 1.15  | 1.179                          | 0.152                                       | 2.85   |
| 2     | 1.154                          | 0.143                                       | 2.86   |
| 2.74  | 1.237                          | 0.187                                       | 2.47   |

correlation function. An example of our calculations is illustrated in Fig. 8(b) and the maximum values at the freezing density at various temperatures are summarized in Table V. Although the required value is not exactly obtained, in most cases the deviation is relatively small.

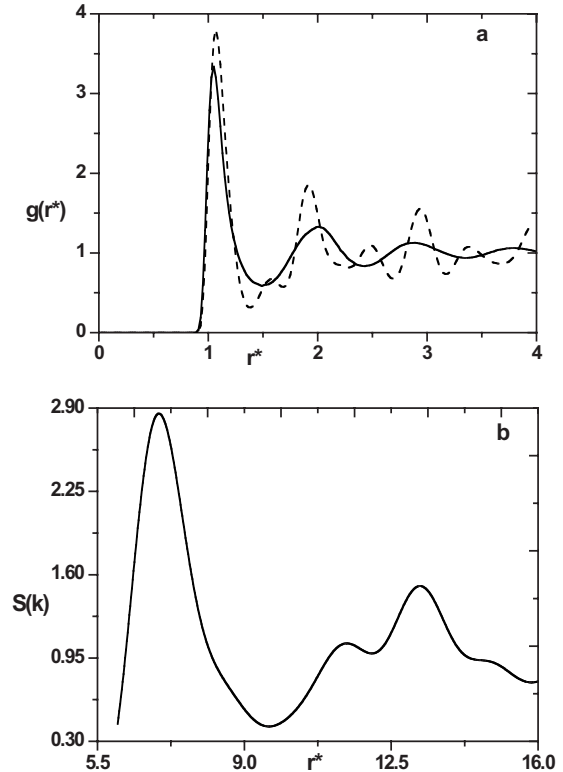


FIG. 8. (a) Comparison of radial distribution functions at  $T^* = 1.0$  for the WCA fluid at freezing (solid line) and melting (dashed line) points. (b) A typical structure factor curve for the WCA fluid at a freezing point ( $\rho^* = 0.98$ ,  $T^* = 1.15$ ).

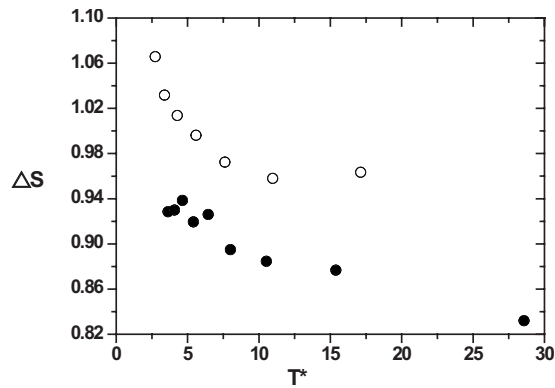


FIG. 9. Comparison of entropy of fusion obtained in this work (●) for the WCA fluid with the data for the Lennard-Jones potential (○) [15].

### F. Entropy of fusion

The simulation data for the change in enthalpy (Tables II and III) allow us to calculate the entropy of fusion, i.e.,  $\Delta S = \Delta H/T$  (Fig. 9). It is evident that for  $T < 10$ , there is a steep increase in  $\Delta S$ , which reflects the high degree of order of the solid phase compared with higher temperatures which approach a constant value. Figure 9 also compares  $\Delta S$  for the LJ and WCA potentials and it is evident that the WCA values are lower at all temperatures. The average value of entropy change calculated was  $\Delta S = 1.20$  with a variation of about 14%, which compares with an average value of 1.36 calculated from the LJ data of Agrawal and Kofke [15]. For a real substance such as aluminum the value of the calculated [37] entropy change is  $\Delta S = 1.2$  compared to an experimental value of  $\Delta S = 1.4$ .

We note that, because of the way the reduce constants are defined, the value of the entropy of fusion can be transformed into real units by simply multiplying the reduced value by the Boltzmann constant. This means that the entropy of fusion predicted by the WCA, Lennard-Jones, and other such two-parameter potentials is independent of the

value of the potential parameters. This provides a convenient way of directly comparing different intermolecular potentials with each other. More importantly, if experimental entropy of fusion data are available for comparison, this insight allows us to quickly assess how accurately an intermolecular potential is likely to predict the thermodynamic properties of real fluids at any temperature.

### IV. CONCLUSIONS

A combination of two molecular simulation algorithms has been used to determine the solid-liquid coexistence of the WCA fluid from low temperatures up to very high temperatures. At very high temperatures, the coexistence pressure approaches the same 12th-power soft-sphere asymptote as the 12–6 Lennard-Jones potential. However, in contrast to the Lennard-Jones potential, which shows a discontinuity of pressure at low temperatures, the coexistence pressure of the WCA potential approaches the zero-temperature limit. Solid-liquid coexistence of the WCA potential commences at densities close to the limiting packing fraction of hard spheres, whereas the triple point is the commencement point for the Lennard-Jones fluid. Three empirical relationships are determined to accurately reproduce the coexistence pressure and both solid and liquid phase densities from near zero temperature up to the very high temperatures. The simulation data are used to reparametrize the Heyes and Okumura WCA equation of state, resulting in considerably greater accuracy for the compressibility factor. The Lindemann and Raveché *et al.* melting rules can be used to predict the onset of melting and the Hansen and Verlet freezing rule can be applied for crystallization.

### ACKNOWLEDGMENTS

We thank the Australian Partnership for Advanced Computing (APAC) for a generous allocation of computing time. One of the authors (A.A.) thanks Swinburne University of Technology for support.

- 
- [1] J. D. Weeks, D. Chandler, and H. C. Andersen, *J. Chem. Phys.* **54**, 5237 (1971).  
 [2] M. Kröger, *Models for Polymeric and Anisotropic Liquids* (Springer, Berlin, 2005).  
 [3] M. Kröger, *Phys. Rep.* **390**, 453 (2004).  
 [4] J. T. Bosko, B. D. Todd, and R. J. Sadus, *J. Chem. Phys.* **121**, 1091 (2004).  
 [5] J. T. Bosko, B. D. Todd, and R. J. Sadus, *J. Chem. Phys.* **124**, 044910 (2006).  
 [6] R. J. Sadus, *Molecular Simulation of Fluids: Theory, Algorithms, and Object Orientation* (Elsevier, Amsterdam, 1999).  
 [7] D. Chandler, J. D. Weeks, and H. C. Andersen, *Science* **220**, 787 (1983).  
 [8] Y. Tang, *J. Chem. Phys.* **116**, 6694 (2002).  
 [9] S. Hess, M. Kröger, and H. Voigt, *Physica A* **250**, 58 (1998).  
 [10] A. de Kuijper, J. A. Scouten, and J. P. Michels, *J. Chem. Phys.* **93**, 3515 (1990).  
 [11] J.-P. Hansen and L. Verlet, *Phys. Rev.* **184**, 151 (1969); *Phys. Rev. A* **2**, 221 (1970).  
 [12] G. C. McNeil-Watson and N. Wilding, *J. Chem. Phys.* **124**, 064504 (2006).  
 [13] E. A. Mastny and J. J. de Pablo, *J. Chem. Phys.* **122**, 124109 (2005); **127**, 104504 (2007).  
 [14] J. Ge, G.-W. Wu, B. D. Todd, and R. J. Sadus, *J. Chem. Phys.* **119**, 11017 (2003).  
 [15] D. A. Kofke, *J. Chem. Phys.* **98**, 4149 (1993); R. Agrawal and D. A. Kofke, *Mol. Phys.* **85**, 43 (1995).  
 [16] D. R. Nelson and B. I. Halperin, *Phys. Rev. B* **19**, 2457 (1979).  
 [17] W. G. Hoover and F. H. Ree, *J. Chem. Phys.* **49**, 3609 (1968).  
 [18] J. K. Johnson, J. A. Zollweg, and K. E. Gubbins, *Mol. Phys.* **78**, 591 (1993).

- [19] L. Wang and R. J. Sadus, Phys. Rev. E **74**, 031203 (2006).
- [20] A. Ahmed and R. J. Sadus, J. Chem. Phys. **131**, 174504 (2009).
- [21] D. J. Evans and G. P. Morriss, *Statistical Mechanics of Non-equilibrium Liquids*, 2nd ed. (Academic Press, London, 2008).
- [22] D. J. Evans, W. G. Hoover, B. H. Failor, B. Moran, and A. J. C. Ladd, Phys. Rev. A **28**, 1016 (1983).
- [23] C. W. Gear, *Numerical Initial Value Problems in Ordinary Differential Equations* (Prentice-Hall, Englewood Cliffs, NJ, 1971).
- [24] H. J. M. Hanley and D. J. Evans, J. Chem. Phys. **76**, 3225 (1982).
- [25] J. R. Morris and X. Song, J. Chem. Phys. **116**, 9352 (2002).
- [26] D. C. Wang and A. P. Gast, J. Phys.: Condens. Matter **11**, 10133 (1999).
- [27] W. G. Hoover, S. G. Gray, and K. W. Johnson, J. Chem. Phys. **55**, 1128 (1971).
- [28] M. A. van der Hoef, J. Chem. Phys. **113**, 8142 (2000).
- [29] D. M. Heyes and H. Okumura, J. Chem. Phys. **124**, 164507 (2006).
- [30] L. Verlet and J. J. Weis, Phys. Rev. A **5**, 939 (1972).
- [31] J. Kolafa and I. Nezbeda, Fluid Phase Equilib. **100**, 1 (1994).
- [32] N. F. Carnahan and K. E. Starling, J. Chem. Phys. **51**, 635 (1969).
- [33] F. A. Lindemann, Phys. Z. **11**, 609 (1910).
- [34] S.-N. Luo, A. Strachan, and D. C. Swift, J. Chem. Phys. **122**, 194709 (2005).
- [35] N. W. Ashcroft and J. Lekner, Phys. Rev. **145**, 83 (1966); N. W. Ashcroft and D. C. Langreth, *ibid.* **159**, 500 (1967).
- [36] H. J. Raveché, R. D. Mountain, and W. B. Streett, J. Chem. Phys. **61**, 1970 (1974).
- [37] J. R. Morris, C. Z. Wang, K. M. Ho, and C. T. Chan, Phys. Rev. B **49**, 3109 (1994).